International Journal of Thermal Sciences 109 (2016) 81–89

Contents lists available at ScienceDirect

International Journal of Thermal Sciences

journal homepage: www.elsevier.com/locate/ijts

Thermal wave propagation through nanofilms in ballistic-diffusive regime by Monte Carlo simulations

Dao-Sheng Tang (唐道胜), Yu-Chao Hua (华钰超), Bing-Yang Cao (曹炳阳)*

Key Laboratory of Thermal Science and Power Engineering of Ministry of Education, Department of Engineering Mechanics, Tsinghua University, Beijing 100084, PR China

ARTICLE INFO

Article history:
Received 30 March 2016
Received in revised form
27 May 2016
Accepted 28 May 2016

Keywords:
Thermal wave
Ballistic-diffusive transport
Monte Carlo simulation
Boundary phonon emission
Overshooting phenomena

ABSTRACT

Investigations on ultrafast heat conduction are of great importance not only for the theoretical understanding of thermal transport, but also the applications of ultra-short pulse laser including the micromachining and the measurements of thermophysical properties of micro/nanomaterials where phonons propagate in ballistic-diffusive regime. In this work, the thermal wave in phonon ballistic-diffusive regime is systematically studied by the Monte Carlo (MC) simulation method. Simulation results show significant influence of the phonon boundary emission conditions, i.e. boundary conditions of phonon Boltzmann transport equation (BTE), on the thermal wave propagation. The MC simulations with phonon Lambert emission (LE) predict a dispersive dissipative thermal wave while the MC simulations with directional emission (DE) predict a non-dispersive dissipative thermal wave. Temperature peak in the MC simulations with LE damps more rapidly than that in DE cases, and heat flux in MC simulations with DE damps exponentially while that in with LE does not. Dispersion relations and wave vector spectrums of thermal waves are determined by the phonon boundary emission, proven by theoretical analyses based on the phonon BTE. The indexes of energy mean square displacement (MSD) relation with respect to time are larger than 1 but less than 2 and decrease as time increases, showing that phonons propagate in ballistic-diffusive regime and evolve from ballistic to diffusive. Effects of the reflection boundary on thermal wave propagation are also investigated and it is found that the temperature overshooting phenomena, due to the wave propagation of heat, is significantly influenced by the properties of both emission and reflection boundaries.

1. Introduction

Wide applications of the ultra-short pulse laser technique in micromachining [1,2] and thermophysical property measurements [3–6] make the studies on ultrafast heat conduction necessarily essential. In general, heat conduction is described by the classical Fourier's law which implies that heat propagates in diffusive regime [7]. However, for ultrafast heat conduction, Fourier's law predicts an infinite speed of heat propagation due to its diffusive feature, deviating from the experimental results which show that heat propagates as thermal waves (or heat waves) [8,9]. When the characteristic time and length of the thermal transport are comparable to the phonon relaxation time and phonon mean free path respectively, phonons propagate also as thermal waves in ballistic-diffusive regime [10].

In the past decades, there are many theoretical and modelling researches on the ultrafast thermal transport. Cattaneo [11] and Vernotte [12] proposed a new constitutive heat conduction model (C-V model) by adding the derivation term of the heat flux to time to Fourier's law. The C-V model predicts the wave propagation of heat. Jeffrey [8] extended the C-V model with a more complex integral kernel. Tzou [9] considered the mutual delay between the heat flux and the temperature and proposed the dual-phase-lagging (DPL) model. By using the DPL model [13,14] and the hyperbolic heat conduction model [15], temperature overshooting phenomena at the reflection boundary was studied. Recently, Majumdar [16] derived the phonon radiation transport equation based on the phonon Boltzmann transport equation (BTE) by analogy between phonons and photons. Chen [17] put forward the ballistic-diffusive heat conduction equation by solving the phonon

* Corresponding author.
E-mail address: caoby@tsinghua.edu.cn (B.-Y. Cao).

http://dx.doi.org/10.1016/j.ijthermalsci.2016.05.030
1290-0729/

BTE with the modified differential approximation method. Guo et al. [18,19] studied the thermal wave based on the thermomass (TM) theory. By solving the TM model, the C-V model and the DPL model numerically, Zhang et al. [20,21] studied the dispersion and damping of thermal waves. Miranda et al. [22] obtained the constitutive equation between the heat flux and the temperature based on the exact solution of the phonon BTE. Besides, simulation methods, including molecular dynamics (MD) simulation, lattice Boltzmann methods (LBM) and Monte Carlo (MC) simulation, are also used in ultrafast thermal transport researches. Tsai et al. [23] and Kim et al. [24] performed MD simulations on heat propagation in simple lattice and multiwall carbon nanotube respectively, and Yao et al. [25] firstly studied the thermal wave propagation in graphene. Xu et al. [26] performed the LBM simulation on ballistic and non-Fourier thermal transport with laser heating. Lacroix et al. [27] and Hua et al. [28] developed the MC methods for ballistic-diffusive thermal transport respectively to solve the phonon BTE and studied the ultrafast heat conduction in silicon nanofilms.

Based on the phonon BTE, it is required for heat wave propagation that phonon quasi-momentum is kept during the transport process (called momentum condition) and no dispersion (or limited dispersion) occurs for phonons energy (called energy condition). For the momentum condition, it is required that phonon scattering process is dominated by the normal phonon-phonon scattering ($\tau_N << t < \tau_R,\tau_B$ where t is the characteristic time of thermal transport andτ_N,τ_R,τ_B are phonon relaxation time for normal scattering process, resistive scattering process and phonon-boundary scattering processes, respectively) or phonons propagate in ballistic regime ($t << \tau_N,\tau_R,\tau_B$). These two cases correspond to two kinds of thermal waves [29]: the second sound [30–33] and the ballistic thermal wave [25,28,29,34] respectively. However, these two kinds of thermal waves are not distinguished clearly in the existing models [8,9,11,12,18–20]. For single-crystal semiconductor under room temperature, when phonon relaxation time and phonon mean free path are in the order of picoseconds and nanometers respectively, the momentum condition is satisfied for ballistic thermal wave in ultrafast heat conduction. While the energy condition is important for the presence of the thermal wave, it has not been discussed yet.

Here, we firstly investigate the ballistic thermal wave (the thermal wave in phonon ballistic-diffusive transport) by directly solving the phonon BTE (only phonon resistive scattering term is taken into consideration) with the MC method. A study on the propagation of the ultra-short heat pulse in single-crystal silicon naonfilms is carried out, and comprehensive understanding on the thermal wave are obtained with systematic analyses on temperature and heat flux results under same macroscopic boundary condition but different microscopic boundary conditions.

2. Monte Carlo simulation

A Monte Carlo (MC) technique [35,36], which directly solves the phonon BTE by simulating the corresponding physical processes, is adopted in this work. The simulation system is presented in Fig. 1. Both the emission and reflection boundaries are perpendicular to the x direction, and there are no confinements in y- and z-directions. Thus, heat pulse propagates along the x direction. The initial temperature is set to be $T_0 = 300$ K, i.e. room temperature. At the initial moment, $t = 0$, a heat pulse with specific function and period 2 ps is input to the film. Adiabatic boundary conditions are set after the pulse heating for both emission and reflection boundaries, which is a reasonable boundary condition considering the practical cases [3–6]. Phonons in films scatter at the boundaries and are reflected diffusively, and the phonon-phonon scatterings are characterized by the relaxation time approximation, i.e. the isotropic scattering. Phonons emissions at the boundary are set to be Lambert emission and directional emission (directional emission in the present work is expressed by the angle θ between the phonon velocity and the x direction).

In ours simulations, the film is divided into 1000 slabs and the number of phonon bundles are set to be 10^8. The temperature is calculated by using its relation with the number of phonons scattered in specific slab and the heat flux is calculated by counting the phonons transmitting the specific position per area and per time. More details can be found in Refs. [28,34–36]. For phonon dispersion relations and frequency spectrum, Debye approximation and gray approximation are adopted respectively [28,37]. The effects of the crystal structure of the single-crystal silicon are not taken into consideration. Phonon velocity v, which is set to be the phonon group velocity v_g in simulations, and the phonon mean free path l are set to be 5000 m/s and 56.2 nm [10], respectively. As a result, the phonon relaxation time of resistive scattering τ_R is 11.2 ps ($\tau_R = l/v_g$). Specific heatc_V and densityρ of the bulk materials are used for the thin film in simulations. The thickness L of the film are set to be 120 nm, 56 nm and 24 nm respectively.

In the present work, we investigate the heat flux pulse condition which has been widely adopted in experimental and numerical studies [3–6,20]. As shown in Fig. 1(a) and (b), the pulse function are selected to be sinusoidal and rectangle functions respectively,

$$q_1 = \begin{cases} q_{max} \times \frac{1}{2}\left(1 - \cos(\omega_{p0} t)\right), & t < t_0 \\ 0, & t \geq t_0 \end{cases} \tag{1}$$

$$q_2 = \begin{cases} q_{max} \times \frac{1}{2}, & t < t_0 \\ 0, & t \geq t_0 \end{cases} \tag{2}$$

where $q_{\max} = 5 \times 10^{11}$ W/m^2, $t_0 = 2$ ps, and $\omega_{p0} = 3.14$ rad ps^{-1}. And the initial conditions are

$$\begin{aligned} T &= T_0, \quad t = 0, 0 \leq x \leq L, \\ q &= 0, \quad t = 0, 0 \leq x \leq L. \end{aligned} \tag{3}$$

3. Results and discussions

3.1. Boundary phonon emission

In analogy to the discussions on surfaces in radiation heat transfer [38] and based on the relevant phonon experiments [39,40], the phonon boundary emissions in MC simulations are set to be the Lambert emission and directional emission respectively. Theoretically, MC simulations are carried out to solve the phonon BTE (under gray approximation)

$$\frac{\partial f}{\partial t} + \mathrm{v} \cdot \nabla f = -\frac{f_0 - f}{\tau_R}. \tag{4}$$

with the boundary condition,

$$f = f_w(t), \tag{5}$$

where f is the phonon distribution function, $f_0 = 1/(\exp(\hbar\omega/k_B T) - 1)$ is the equilibrium phonon distribution function and f_w is the distribution function at the boundary. The boundary emissions in MC simulations correspond to the boundary conditions of the phonon BTE with the following relations [28],

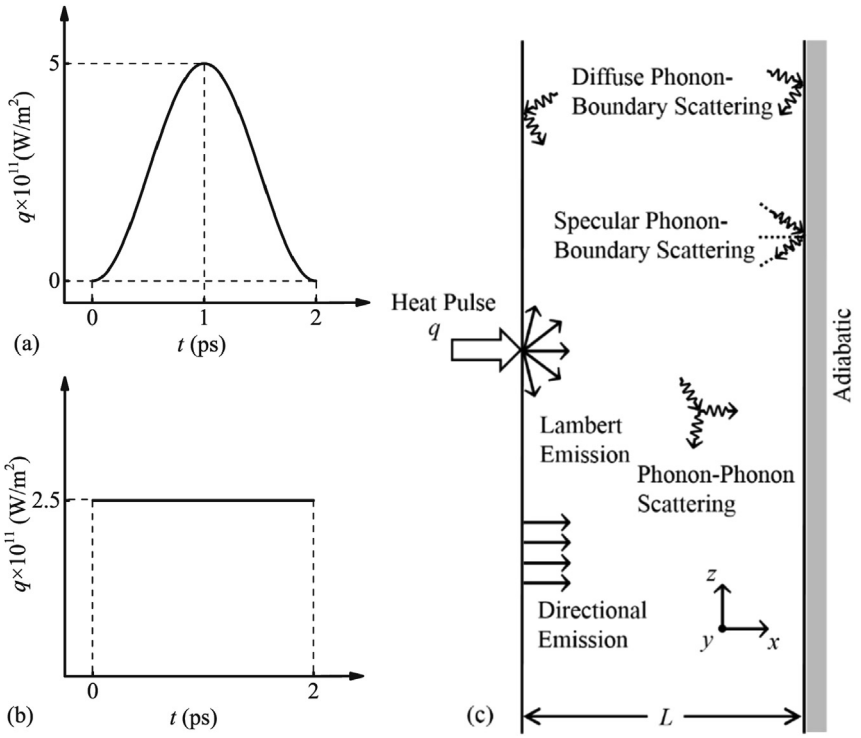

Fig. 1. Schemes of heat pulse and simulation system of thin film. (a) sinusoidal-function heat pulse; (b) rectangular-function heat pulse; (c) simulation system with scattering regime of phonon-phonon and phonon-boundary.

$$G(\theta) = \int_0^{\theta} \rho(\theta')\cos\theta' \sin\theta' \mathrm{d}\theta', \tag{6}$$

where $\rho(\theta')$ is the part of the boundary distribution function relative to the angle only at specific position and $G(\theta)$ is the random quantity distributing from 0 to 1 uniformly which is namely the emission function in MC simulations. Thus, the Lambert phonon emission corresponds to the boundary condition of the equilibrium distribution function $f = f_0$ while the directional phonon emission corresponds to that of a delta function $f = F\delta(\vec{k} - \vec{k}_0)$ in which F is the total phonon number, $\vec{k}$ and $\vec{k}_0$ are phonon wave vectors. More details of the relevance between emission settings (microscopic boundary conditions) and macroscopic boundary condition could be found in Ref. [29].

3.2. Temperature and heat flux evolution

As shown in Fig. 2, the temperature profiles with Lambert and directional emissions are both calculated. The propagation time of the heat pulse in calculations is 2–20 ps which are comparable to the phonon relaxation time τ_R (11.2 ps), as a result, the momentum condition of the thermal wave is satisfied. To examine the difference between the different settings of boundary emission, two different kinds of heat pulse, i.e. the sinusoidal-function heat pulse and the rectangular-function heat pulse, are used. The MC simulations with LE and DE predict that the heat pulse propagates with finite speed v_g, i.e. the thermal wave front velocity is v_g, despite of the different phonon boundary emission conditions. Besides, different from the non-dispersive dissipative temperature wave predicted by the MC simulations with DE, the MC simulations with LE predict a dispersive dissipative temperature wave: the shapes of the heat pulse are kept in predictions of the MC simulations with DE but are not in those of the LE cases. As a result, the shape of thermal waves in the DE cases are considerably sensitive to the changes of heat pulse shape at the emission boundary, while in the LE cases the changes of boundary heat pulse shape can only affect the shape of the thermal waves within the first 5 ps. Besides, we plot the temperature profiles with respect to time at specific locations in Fig. 3(a) and (b). The predictions of the classical thermal wave model, i.e. the C-V model,

$$q + \tau_{CV}\frac{\partial q}{\partial t} = -k\nabla T, \tag{7}$$

where τ_{CV} is the relaxation time of the heat flux to temperature gradient and k the thermal conductivity, are also plotted as comparisons. At the front surface ($x = 0$ nm), the shapes of temperature profiles by the MC simulations and the C-V model are nearly the same, especially for the profiles by the MC simulation with LE and the C-V model, even though their maximum magnitudes are different. However, those at x=28 nm show that the MC simulations with DE and LE and the C-V model predict quite different results. The MC simulations with DE and the C-V model both predict the prominent wave nature of the heat propagation. However, they predict the different velocities of thermal waves, which is shown by that the MC simulations with DE predict a more rapid temperature response. The MC simulations with LE predict a lower temperature peak and wider temperature-time profile which is different from those of the MC simulations with DE and the C-V model in shape. It could be concluded that the effect from the boundary emission occurs during the propagation of heat pulse.

Fig. 4 shows the maximum temperature-time profiles predicted by the MC simulations with DE and LE and the C-V model. The MC simulations with LE predict a more severe damping compared with the MC simulations with DE. In predictions of MC simulations with

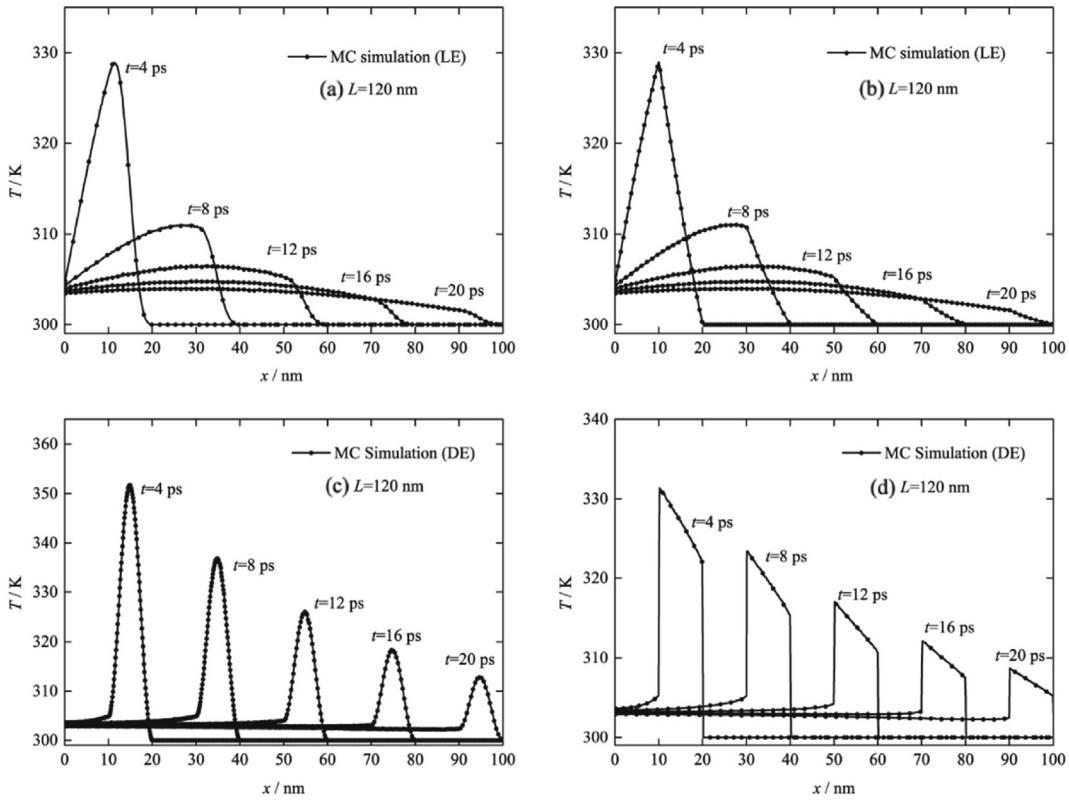

Fig. 2. Temperature results of MC simulations with LE under (a) sinusoidal-function heat pulse; (b) rectangular-function heat pulse and MC simulations with DE under (c) sinusoidal-function heat pulse; (d) rectangular-function heat pulse.

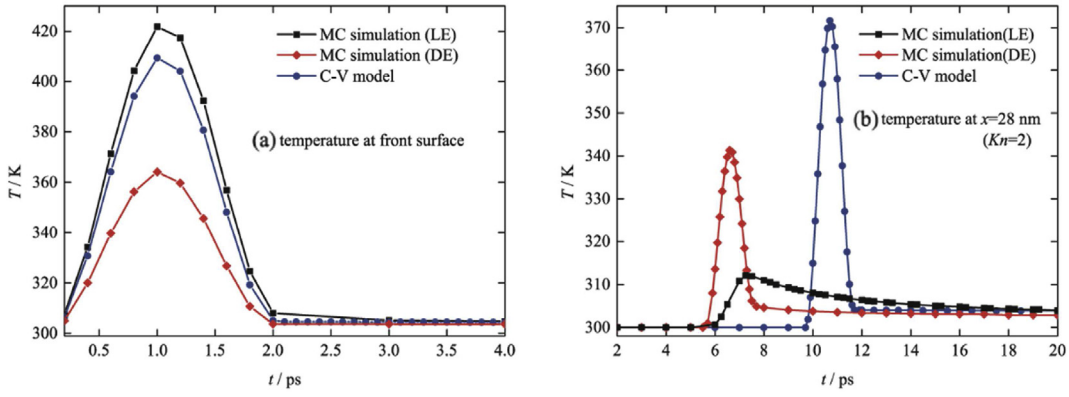

Fig. 3. Temperature profiles with respect to time at: (a) front surface and (b) $x = 28$ nm.

DE and the C-V model, the heat pulse propagates as a non-dispersive wave with energy being focused, and the phonon-phonon scattering (the attenuation term in the C-V model) is the only reason causing the damping of the temperature peak. However, in the LE cases, the heat pulse disperses and energy tends to distribute uniformly in x-direction during the propagation, leading to the damping of the temperature peak. As the scattering processes are not inadequate in the first several picoseconds, the dispersion is the main reason that should be responsible for the damping of the temperature peak in the LE case.

In order to have an intuitive understanding on the damping of thermal waves, the damping of the heat flux is calculated with the method used in Ref. [21]. In this method, the definitions of the damping factor and damping level are

$$\xi = L_d/\sqrt{\alpha\tau_R} \tag{8}$$

$$\varepsilon_q = \frac{q\left(x_{p0}^q\right) - q\left(x_{p0}^q + L_d\right)}{q\left(x_{p0}^q\right)} \tag{9}$$

respectively. x_{p0}^q is the reference location (the location of the reference wave front), L_d is the distance between the current wave front and the reference wave front, $q(x_{p0}^q)$ and $q(x_{p0}^q + L_d)$ are the max values of the reference heat flux wave and the current heat flux wave respectively, and α is the thermal diffusivity. As shown in Fig. 5(a) and (b), the $-\ln(1 - \varepsilon_q)$ vs. ξ profiles for MC simulations

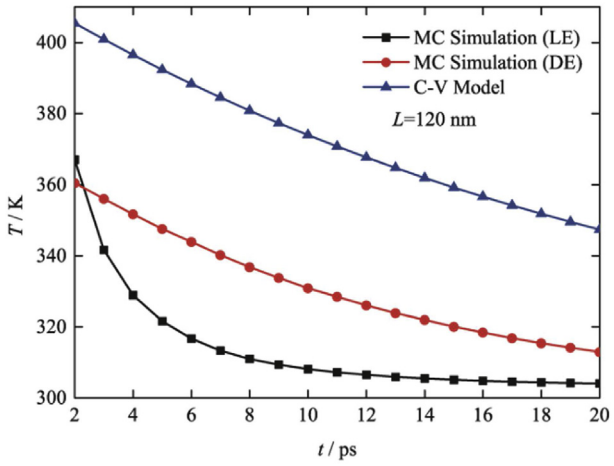

Fig. 4. Temperature peak profiles with respect to time.

with DE and LE and the C-V model are obtained. Good linearity of the profiles of the MC simulations with DE and the C-V model indicates that heat flux damps as exponential function. Theoretically, the exponential damping results from that the resistive scattering probability function is an exponential function. However, the MC simulations with LE predict a nonlinear $-\ln(1-\varepsilon_q)$ vs. ξ profile and a more severe damping of the heat flux. This could be explained as the result of the dispersion of the thermal wave as we mentioned above. The slopes of the profiles by the MC simulations with DE and the C-V model are different. Actually, the thermal diffusivity in the MC simulations with DE should be

$$\alpha = \frac{k}{\rho c_V} = vl, k = \rho c_V vl, \tag{10}$$

while the thermal diffusivity in the C-V model is

$$\alpha = \frac{k}{\rho c_V} = \frac{1}{3}vl,\ k = \frac{1}{3}\rho c_V vl. \tag{11}$$

which is because that $v_x^2 = 1/3v_g^2$, $v_x = v_g\cos(\theta)$, the diffusive approximation is used in the C-V model while $v_x^2 = v_g^2$ in the MC simulation with DE due to the directional emission. As a result, the damping factor for the C-V model and the MC simulations with DE can be simplified as

$$\xi_{\mathrm{CV}} = \frac{\sqrt{3}}{Kn}, \tag{12}$$

and

$$\xi_{\mathrm{MC\text{-}DE}} = \frac{1}{Kn}. \tag{13}$$

respectively. Plotting the $-\ln(1-\varepsilon_q)$ vs. ξ profile of the MC simulations with DE with damping factor $\xi = 3/Kn$, the similar profile with that of the C-V model is then obtained, which is shown in Fig. 5(a).

To have an analytical understanding on the boundary emission and thermal waves, dispersion relations and wave vector spectrums of thermal waves predicted by the MC simulations with both LE and DE are analyzed. Considering the phonon BTE without scattering term,

$$\frac{\partial f}{\partial t} + v_g\cos(\theta)\frac{\partial f}{\partial x} = 0, \tag{14}$$

the dispersion relation of distribution function [29],

$$\omega_t = v_g\cos(\theta)k_t, \tag{15}$$

can be obtained from the formal solution $f(x - v_g\cos(\theta)t)$ which is a wave solution. ω_t is the angular frequency of the thermal wave and k_t is the wave vector. As the temperature have a linear relation with the distribution function under gray approximation and the assumption that the heat capacity is constant, the dispersion relations for both two are the same. Thus, the dispersion relation for thermal wave of MC simulations with LE is

$$\omega_t = v_g\cos(\theta)k_t,\ 0^\circ < \theta < 90^\circ, \tag{16}$$

and θ distributes according to the Lambert cosine law. As a special case, the dispersion relation for thermal wave of MC simulations with DE is

$$\omega_t = v_g\cos(\theta)k_t,\ \theta = \theta_0, \tag{17}$$

where θ_0 is set to be zero in this work. Wave vector spectrums of thermal waves are shown in Fig. 6(a) and (b), the proportion for specific wave vector can be calculated according to the distribution of the angle which is a cosine-function for Lambert emission and a delta function for directional emission. Difference between the two

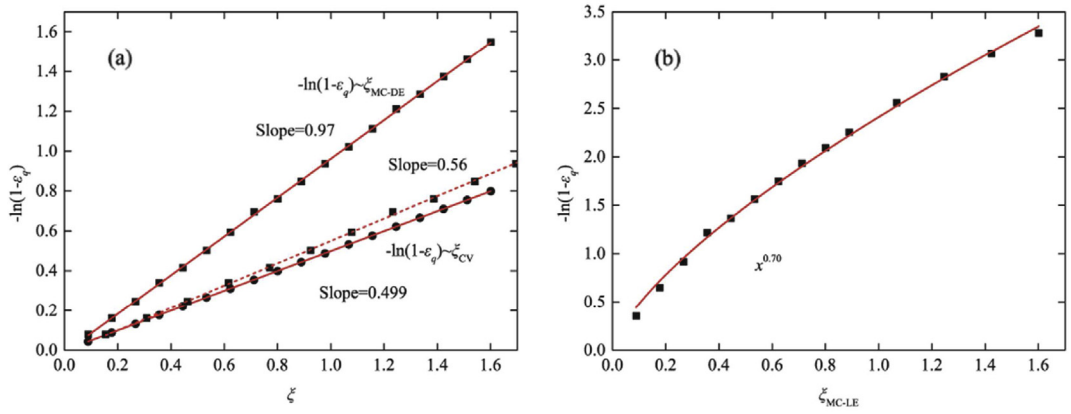

Fig. 5. Damping of the heat flux. (a) $-\ln(1-\varepsilon_q)$ vs. ξ profiles of the MC simulation with DE and the C-V model, the dash line is the $-\ln(1-\varepsilon_q)$ vs. ξ profile of the MC simulation with DE where ξ is set to be $3/Kn$; (b) $-\ln(1-\varepsilon_q)$ vs. ξ profiles of the MC simulation with LE.

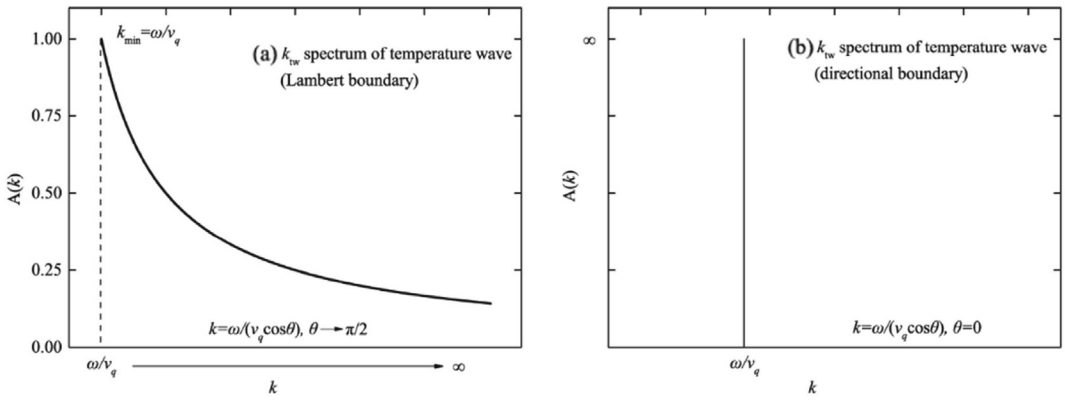

Fig. 6. Wave vector spectrums of thermal waves predicted by MC simulation with (a) LE and (b) DE.

wave vector spectrums is obvious: there is no upper bound for the wave vector of the thermal wave in MC simulation with LE while there are both upper and lower bounds for that in MC simulations with DE. It is just the broader distribution of the wave vector spectrum in MC simulations with LE that weakens of the wave propagation of heat. In a word, temperature results corresponding to the two wave vector spectrums show the requirement for thermal wave propagation in energy aspect, i.e. the energy condition: there should be no dispersion during the propagation of the heat pulse.

Energy mean square displacement (MSD) profiles with respect to time is calculated to investigate regime of phonon transport. The definition of energy MSD is [41]

$$\sigma^2(t)=\frac{\int (E(x,t)-E_0)(x-x_0)^2\mathrm{d}x}{\int (E(x,t)-E_0)\mathrm{d}x}, \tag{18}$$

where x is the position, x_0 is the position of heat pulse, $E(x,t)$ is the internal energy of the film at time t and position x, E_0 is the initial internal energy of the thin film. From the MSD-time relations, we can deduce the regime of phonon transport with the following rule [41],

$$<\sigma^2(t)> \sim \begin{cases} t, & \text{diffusive} \\ t^{\alpha}(1<\alpha<2), & \text{ballistic-diffusive} \\ t^2, & \text{ballistic} \end{cases} \tag{19}$$

where <.> means ensemble averaging. MSD-time relations for MC simulation with DE and LE (under excitation of sinusoidal pulse) are shown in Fig. 7(a) and (b). The indexes in MC simulations with LE, i.e. 1.88, 1.68 and 1.58 respectively, are larger than 1 but less than 2, and decrease as time increases, showing that thermal wave propagates in phonon ballistic-diffusive regime and this regime is evolved from ballistic to diffusive with enough resistive scatterings happening. MC simulations with DE predict the same rule of the regime of phonon propagation and its evolution, however, the indexes are different. At the same time interval, indexes in MC simulation with LE are larger than those in MC simulation with DE correspondingly, which may result from the different scattering space distributions and back-scatterings with emission boundary in both cases.

3.3. Reflection boundary and overshooting phenomena

Effect of the reflection boundary on the propagation of the thermal wave is investigated in this section. We simulate the thermal wave propagation in 24-nm- and 56-nm-thick films with two boundary settings: one is the Lambert emission boundary with diffuse reflection boundary, and the other is the directional emission boundary with specular reflection boundary. For thermal wave propagation in nanofilms, specular reflection would not make a difference when the incident phonons are not directional (the angles of the incident phonons have distributed nearly uniformly in wave vector space due to the Lambert emission and few scatterings), and diffuse reflection (with directional emission) could be equivalent to the Lambert emission. As a result, we select the combinations of Lambert emission with diffuse reflection and

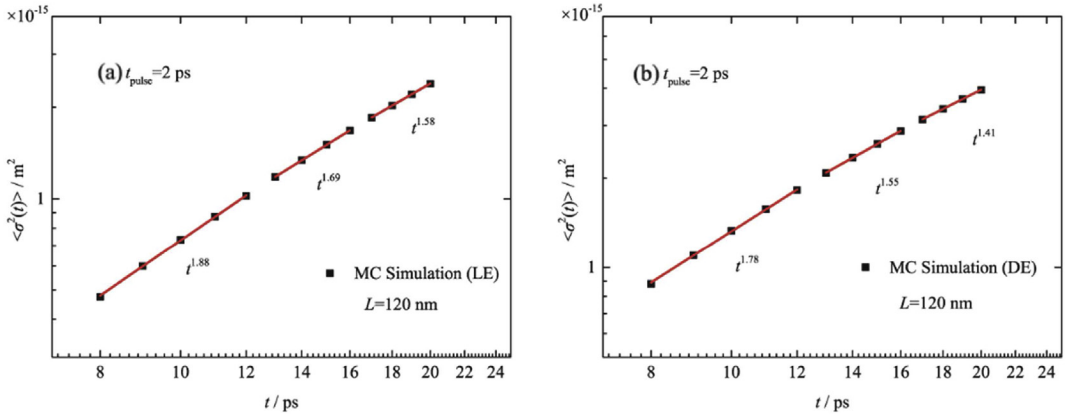

Fig. 7. MSD-time relations in MC simulation with (a) LE and (b) DE.

directional emission with specular reflection. The character times τ_B for phonon-boundary scattering in nanofilms of two thicknesses are 4.8 ps and 9.6 ps (we calculate $\tau_B = L/v_g$) respectively, and they are both smaller than τ_R(11.2 ps) and comparable to the calculation time. As a result, the temperature and heat flux results would be not only influenced by the phonon resistive scattering but also the phonon-boundary scattering.

Temperature profiles by the MC simulations with LE and DE shown in Figs. 8 and 9 predict an overshooting temperature at the reflection boundary. As what have been confirmed in section 3.2, phonons propagate in ballistic-diffusive regime with inadequate scatterings in films. The temperature overshooting phenomena occurs in phonon ballistic-diffusive transport accompanying with the occurrence of thermal waves. At $t = 6$ ps in the 24-nm-thick film and $t = 12$ ps in the 56-nm-thick film, thermal waves arrive the reflection boundary and overshooting temperature appears: new temperature peaks, present at the boundary, are higher than the ambient temperature, and even higher than the previous temperature peak in the 24-nm-thick film. Correspondingly, negative heat flux is presented at the boundary, shown in Fig. 10. After the reflection by the boundary, thermal waves propagate in the opposite direction and the overshooting temperature disappears. The temperature overshooting phenomena shown in the 24-nm-thick film is more significant than that shown in the 56-nm-thick film, which is illustrated in Figs. 8 and 9. That is because proportion of the ballistic transport decreases and proportion of the diffusive transport increases in the 56-nm-thick film compared with phonon propagation in the 24-nm-thick film. The reversion of the heat conduction direction, indicated by the negative heat flux, results from the confinement of the reflection boundary. Before the emission phonons met the reflection boundary, ballistic transport always enhance the heat conduction in transient case, however, once phonons in ballistic regime scatter at the boundary, the confinement on phonon free path would appear. The phonon scatterings with reflection boundary are totally resistant for emission phonons whose direction are all positive.

Theoretically, the overshooting phenomena of temperature is the result of the wave propagation of heat. The waves are reflected once they met the wall during the propagation. While the waves are of finite period, reflecting part and propagating part are superposed in amplitudes. This perspective is confirmed by the simulation results that the overshooting phenomena is significant when heat propagates as a non-dispersive wave, shown in Fig. 9. Due to the dispersion of thermal waves in MC simulations with LE, the energy of thermal waves disperses, causing that the overshooting phenomena in MC simulations with LE is not as significant as that in MC simulations with DE, which is illustrated by Fig. 8. While the specular reflection boundary do not change the absolute value of the angle of phonons but the direction of propagation only, the non-dispersive thermal wave is kept after reflection and overshooting phenomena is significant. For diffuse reflection boundary, while the thermal wave has been a dispersive wave due to the Lambert emission, diffuse reflection exacerbates the dispersion and causes the overshooting phenomena even weaker. As the overshooting phenomena is the result of the wave propagation of heat, it may also occur accompanying with the other kind of thermal wave phenomena, i.e. the second sound, in a larger spatial scale, which will be studied in the following works.

4. Concluding remarks

In this work, we study the thermal wave in phonon ballistic-diffusive transport regime by the MC simulation method. Comprehensive understanding on the ballistic thermal wave is

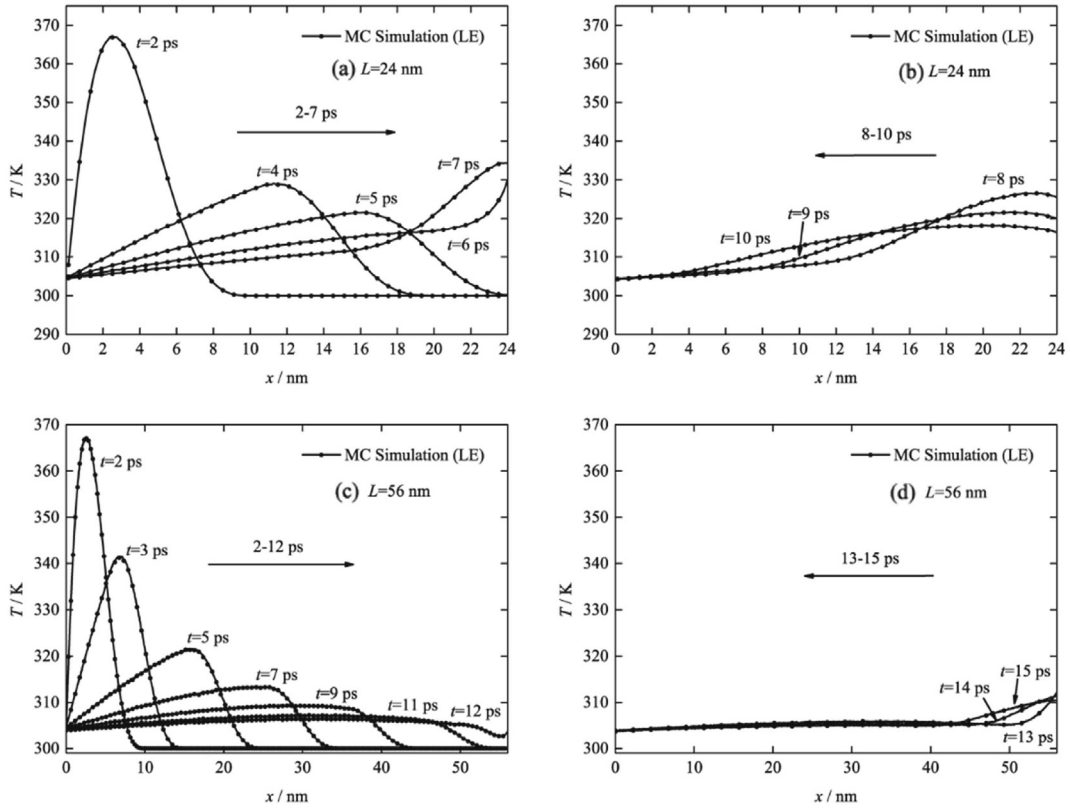

Fig. 8. Temperature profiles in (a) 24-nm-thick film ($t = 2$–7 ps); (b) 24-nm-thick film ($t = 8$–10 ps); (c) 56-nm-thick film ($t = 2$–12 ps) and (d) 56-nm-thick film ($t = 13$–15 ps): the Lambert emission boundary and diffuse reflection boundary.

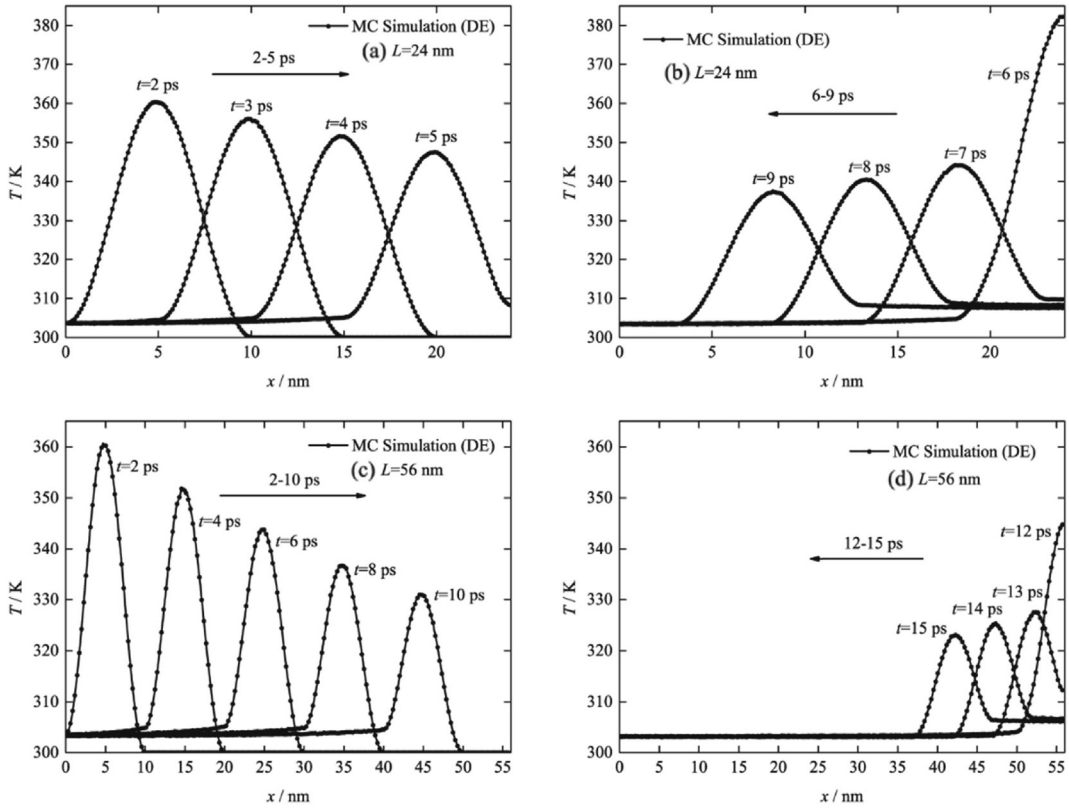

Fig. 9. Temperature profiles in (a) 24-nm-thick film ($t = 2–5$ ps); (b) 24-nm-thick film ($t = 6–9$ ps); (c) 56-nm-thick film ($t = 2–10$ ps) and (d) 56-nm-thick film ($t = 12–15$ ps): the directional emission boundary and specular reflection boundary.

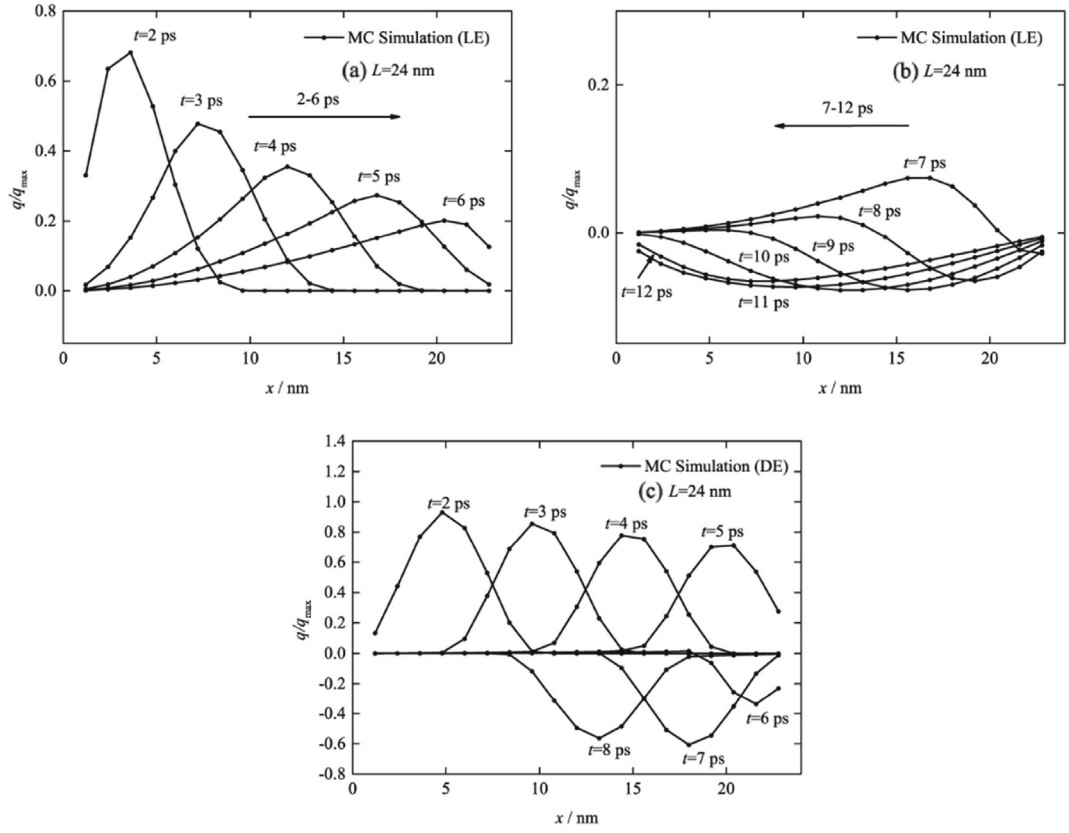

Fig. 10. Heat flux profiles in 24-nm-thick film predicted by MC simulations with (a) LE ($t = 2–6$ ps); (b) LE ($t = 7–12$ ps) and (c) DE ($t = 2–8$ ps).

obtained with calculations on the temperature and heat flux profiles with and without reflection boundary, energy MSD-time relations and damping of the heat flux.

Heat propagates in a finite speed equal to phonon group velocity. Boundary emissions are of great influence on the temperature and heat flux profiles, energy MSD-time relations and damping of the heat flux in MC simulations for ultrafast thermal transport. The MC simulations with DE predict a non-dispersive dissipative thermal wave while the MC simulations with LE predict a dispersive dissipative thermal wave, which results in a faster decline of the max-temperature and max-heat flux in the MC simulations with LE. Indexes of the energy MSD-time relations in LE case are always larger than those in the DE case which may result from the different spatial distributions of phonon scatterings and different back-scatterings with boundary.

Indexes of the energy MSD-time relations are calculated to be greater than 1 but less than 2, showing that phonons propagate in ballistic-diffusive regime when the characteristic time of thermal transport is comparable with the phonon relaxation time. Diffusive transport tends to share more proportion in phonon propagation as time increases due to the increase of the resistive scatterings.

Overshooting phenomena occurs in phonon ballistic-diffusive transport accompanying with the thermal wave phenomena. The more proportion the diffusive transport shares, and the more severely dispersive the thermal wave is (i.e. the weaker the wave propagation of heat in other words), the less significant the overshooting phenomena is, which proves that wave propagation of heat is the reason why overshooting phenomena occurs. Overshooting phenomena may also occur in second sound in a larger spatial scale, which will be further investigated in the future.

Acknowledgments

This work is financially supported by National Natural Science Foundation of China (Nos. 51322603, 51136001, 51356001), Science Fund for Creative Research Group (No. 51321002), and the Tsinghua National Laboratory for Information Science and Technology of China (TNList).

References

[1] Cahill G, Ford WK, Goodson KE, Mahan GD, Majumdar A, Maris HJ, et al. Nanoscale thermal transport. J Appl Phys 2003;93:793.
[2] Cheng J, Liu CS, Shang S, Liu D, Perrie W, Dearden G, et al. A review of ultrafast laser materials micromachining. Opt Laser Tech 2013;46:88.
[3] Costescu RM, Wall MA, Cahill DG. Thermal conductance of epitaxial interfaces. Phys Rev B 2003;67:054302.
[4] Koh YK, Singer SL, Kim W, Zide JMO, Liu H, Cahill DG, et al. Comparison of the 3ω method and time-domain thermoreflectance for measurements of the cross-plane thermal conductivity of epitaxial semiconductors. J Appl Phys 2009;105:054303.
[5] Koh YK, Cao Y, Cahill DG, Jena D. Heat-transport mechanisms in superlattices. Adv Funct Mater 2009;19:610.
[6] Feser JP, Cahill DG. Probing anisotropic heat transport using time-domain thermoreflectance with offset laser spots. Rev Sci Instrum 2012;83:104901.
[7] Fourier J. Analytical theory of heat. New York: Dover Publications; 1955.
[8] Joseph DD, Preziosi L. Heat waves. Rev Mod Phys 1989;61:41.
[9] Tzou DY. Macro- to micro-scale heat transfer: the lagging behavior. Washington, DC: Taylor and Francis; 1997.
[10] Chen G. Nanoscale energy transport and conversion: a parallel treatment of electrons, molecules, phonons, and photons. Oxford University Press; 2005.
[11] Cattaneo C. Atti Sem Mat Fis Univ Modena 1948;3:83.
[12] Vernotte MP, Hebd CR. Paradoxes in the continuous theory of the heat equation. Acad Sci Paris 1958;246:3154.
[13] Jou D, Criado-Sancho M. Thermodynamic stability and temperature overshooting in dual-phase-lag heat transfer. Phys Lett A 1998;248:172.
[14] Al-Nimr M, Naji M, Al-Wardat S. Overshooting phenomenon in the hyperbolic heat conductioin model. Jpn J Appl Phys 2003;42:5383.
[15] Xu MT, Guo JF, Wang LQ, Cheng L. Thermal wave interference as the origin of the overshooting phenomenon in dual-phase-lagging heat conduction. Int J Therm Sci 2011;50:825.
[16] Majumdar A. Microscale heat conduction in dielectric thin film. J Heat Trans 1993;115:7.
[17] Chen G. Ballistic–diffusive heat-conduction equations. Phys Rev Lett 2001;86:2297.
[18] Cao BY, Guo ZY. Equation of motion of a phonon gas and non-Fourier heat conduction. J Appl Phys 2007;102(053503).
[19] Dong Y, Cao BY, Guo ZY. Generalized heat conduction laws based on thermomass theory and phonon hydrodynamics. J Appl Phys 2011;110(063504).
[20] Zhang MK, Cao BY, Guo YC. Numerical studied on dispersion of thermal waves. Int J Heat Mass Trans 2014;67:1072.
[21] Zhang MK, Cao BY, Guo YC. Numerical studies on damping of thermal waves. Int J Therm Sci 2014;84:9.
[22] Ordonez-Miranda J, Yang RG, Alvarado-Gil JJ. A constitutive equation for nano-to-macroscopic-scale heat conduction based on the Boltzmann transport equation. J Appl Phys 2011;109:084319.
[23] Tsai DH, MacDonald RA. Molecular-dynamical study of second sound in a solid excited by a strong heat pulse. Phys Rev B 1976;14:4714.
[24] Kim T, Osman MA, Richards CD, Bahr DF, Richard RF. Molecular dynamic simulation of heat pulse propagation in multiwall carbon nanotubes. Phys Rev B 2007;76:155424.
[25] Yao WJ, Cao BY. Thermal wave propagation in graphene studied by molecular dynamics simulations. Chin Sci Bull 2014;59:3495.
[26] Xu J, Wang XW. Simulation of ballistic and non-Fourier thermal transport in ultra-fast laser heating. Phys B 2004;351:213.
[27] Lacroix D, Joulain K, Lemonnier D. Monte Carlo transient phonon transport in silicon and germanium at nanoscales. Phy Rev B 2005;72:064305.
[28] Hua YC, Dong Y, Cao BY. Monte Carlo simulation of phonon ballistic diffusive heat conduction in silicon nanofilm. Acta Phys Sin 2013;62:244401.
[29] Tang DS, Hua YC, Nie BD, Cao BY. Phonon wave propagation in ballistic-diffusive regime. J Appl Phys 2016;119:124301.
[30] Peshkov V. Second sound in helium II. J Phys Mosc 1944;8:381.
[31] Acherman CC, Bertman B, Fairbank HA, Guyer RA. Second sound in solid Helium. Phys Rev Lett 1966;16:789.
[32] Guyer RA, Krumhansl JA. Thermal conductivity, second sound, and phonon hydrodynamic phenomena in nonmetallic crystals. Phys Rev 1966;148:778.
[33] Zhang P, Murakami M, Wang RZ. Study of the transient thermal wave heat transfer in a channel immersed in a bath of superfluid helium. Int J Heat Mass Trans 2006;49:1384.
[34] Heiblum M, Nathan MI, Thomas DC, Knoedler CM. Direct observation of ballistic transport in GaAs. Phys Rev Lett 1985;55:2200.
[35] Peraud JM, Hadjiconstantinou NG. An alternative approach to efficient simulation of micro nanoscale phonon transport. Appl Phys Lett 2012;101:153114.
[36] Hua YC, Cao BY. Phonon ballistic-diffusive heat conduction in silicon nanofilms by Monte Carlo simulations. Int J Heat Mass Trans 2014;78:755.
[37] Hao Q, Chen Gang, Jeng MS. Frequency-dependent Monte Carlo simulations of phonon transport in two-dimensional porous silicon with aligned pores. J Appl Phys 2009;106:114321.
[38] Howell JR, Siegel R, Menguc MP. Thermal radiation heat transfer. CRC Press, Taylor & Francis Group; 2010.
[39] Sherlock RA, Mills NG, Wyatt AFG. The angular distribution of phonons radiated from a heated solid surface into liquid ^{4}He: II. Cleaved sodium fluoride {100} faces. J Phys C Solid State Phys 1975;8:300.
[40] Tucker MAH, Wyatt AFG. Phonons in liquid ^{4}He from a heated metal film: II. The angular distribution. J Phys Condens Matter 1994;6:2825.
[41] Zhang G, Li BW. Anomalous vibrational energy diffusion in carbon nanotubes. J Chem Phys 2005;123:014705.